ChemPubSoc Europe

DOI: 10.1002/slct.201701303

Chemistry SELECT Full Papers

Energy Technology & Environmental Science

Bioinspired Copper Coordination Polymer Catalysts for Oxygen Reduction Reaction

Rupali Mishra,[a] Bhushan Patil,[b] Ferdi Karadaş,*[a, b] and Eda Yılmaz*[b]

Non–noble metal catalysts have recently emerged as promising alternatives to the expensive platinum catalysts for the oxygen reduction reaction (ORR). In this study, a new domain of materials, copper based coordination polymers, has been investigated as promising catalysts for ORR. The study was inspired by copper incorporating biomolecules, which efficiently catalyse the oxygen reduction reaction in nature. Two coordination polymers, $[Cu_2(\mu-AcO)_4Po)]_n$ (shortened as[Cu–A]) and $[Cu_2(\mu-BzO)_4Po)]_n$ (shortened as[Cu–B]), incorporating one–dimensional chains of Cu(II) paddle wheel units bridged with phosphineoxide ligands were combined with multi–walled carbon nanotubes (MCNTs) to prepare hybrid electrocatalysts for ORR. The electrochemical analysis demonstrates that [Cu–A] catalyses ORR with 3.24 numbers of electrons with Tafel slopes of 122/83 mV dec^{-1} while it is 2.37 numbers of electrons with Tafel slopes of 131/84 mV dec^{-1} for [Cu–B]. Rotating disk electrode measurements and evaluation of Tafel slopes reveal that acetate moieties attached to Cu site shift the onset potential of ORR anodically (ca. 40 mV) compared to the one with benzoate bridging groups. The effect of bridging ligands to the stability and activity of catalysts in alkaline media was also evaluated. This study opens a new perspective for the development of non–platinum ORR catalysts.

Introduction

The oxygen reduction reaction (ORR) is a crucial reaction in numerous applications including fuel cells[1–3] and metal–air batteries.[4,5] Platinum is one of the most efficient electrocatalysts for ORR.[6–10] However, its high cost, scarcity, and tendency of the surface to poison, constrain its applications. This triggers the interest of researchers to develop alternative electrocatalysts for ORR including carbon–based materials such as carbon nanotubes,[11,12] graphene,[13–15] and transition metal compounds such as cobalt,[16,17] iron,[18–21] and copper.[22,23] Cu is a highly abundant element in earth's crust and it is used in a wide range of areas such as host–guest systems,[24–29] catalysis,[30–34] magnetism,[35–39] biological systems,[40–44] and electrochemistry.[45–47]

Cu can also be found in enzymes participating in several reactions. Bio–inspired copper catalysts[48,49] and Cu–based enzymes have been reported to be active catalysts in ORR such as ascorbate oxidase,[50] bilirubin oxidase,[51–54] and laccase[55–59] etc. The use of such enzymes for the practical systems is however, not possible due to the requirement of very limiting operating conditions such as neutral pH, narrow temperature range, and etc. Interestingly, ORR mechanism and potential are different for each biomolecule participating in the process even though they contain copper as the active site reducing the oxygen. This suggests that the ligands attached to Cu have a vital role in the ORR mechanism. During the adsorption and dissociation of O_2 molecules, Cu is significantly affected by the ligands attached to it.

A 1D coordination polymer incorporating copper paddle–wheel units has recently been investigated as an active electrocatalyst for water oxidation.[60] The previous study shows that copper sites in the paddle–wheel unit can activate water to form O_2. Given the microscopic reversibility of ORR and OER mechanisms, the electrocatalytic activity of copper paddle–wheel unit in ORR has been investigated in this work. The previously reported 1D coordination polymer together with a new derivative have been used in the study to investigate the effect of surrounding bridging ligands to the catalytic activity and stability of copper systems.

Result and discussion

Crystal Structure

Copper acetate was reacted with phosphine ligands in methanol/dichloromethane mixture in peroxide media, which results in the formation of dark blue crystals of [Cu–A] and [Cu–B]. The structure of [Cu–A] was already described in our previously reported work.[60] The crystal structure of the new copper catalyst, [Cu–B] was successfully solved in the monoclinic space group, P121/*n*1. Crystallographic data and structural refinement parameters for the compound are given in (Table S1). 1D chain of both compounds consists of independ-

[a] Dr. R. Mishra, Prof. F. Karadaş
Department of Chemistry, Bilkent University, 06800, Ankara, Turkey
[b] Dr. B. Patil, Prof. F. Karadaş, Prof. E. Yılmaz
Institute of Materials Science and Nanotechnology, National Nanotechnology Research Center (UNAM) Bilkent University, 06800, Ankara, Turkey
Tel: + 90-312-290 19 97
Tel: + 90-312-290-8028
Fax: + 90-312-266 40 68
E-mail: karadas@fen.bilkent.edu.tr
yilmaz@unam.bilkent.edu.tr

Supporting information for this article is available on the WWW under https://doi.org/10.1002/slct.201701303

© 2017 Wiley-VCH Verlag GmbH & Co. KGaA, Weinheim

ent copper paddle – wheel units linked by phosphineoxide (P_o) bridging ligands in Figure 1(b). Each metal ion is surrounded by

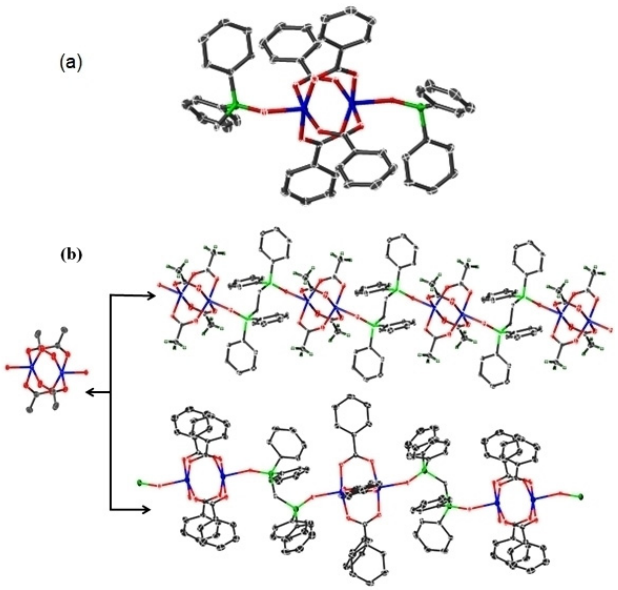

Figure 1. Asymmetric unit of **[Cu–B]** and hydrogen atoms are omitted for clarity in (a). In fig (b) showing both different 1D chains of **[Cu–A]** and **[Cu–B]**.Colour code: Cu = blue; P = green; O = red; C = black.

five oxygen atoms, one of which belongs to oxygen of bis (diphenylphosphino)phosphine dioxide ligand while the remaining four belong to four different benzoate bridging moieties. In [Cu–B], copper centre is in square pyramidal coordination environment Figure 1(a). In both compounds the paddle–wheel units have different metal–to–metal distance. Cu···Cu distance is 2.6224 Å in [Cu–B] and while it is 2.658 Å for [Cu–A]. This difference in the metal–to–metal distance obtained for [Cu–B] could be attributed to the presence of a bulkier bridging group. The crystal packing diagrams of compounds displayed in Figures S3 (a) and (b) clearly indicate that the shortest distance between copper centres in neighbouring chains is much larger for [Cu – B] 8.086 Å for [Cu – A] and 11.104 Å for [Cu – B] as a result of bulky benzoate groups. The supramolecular framework of [Cu – B] is stabilized by C–H···π interactions between H atoms of the phenyl ring of benzoate molecules (2.822–2.848 Å) with other aromatic ring of benzoate groups. The supramolecular structure of [Cu – B] is further form an overall 3D structure in Figure S2 (b). Both compounds show 3D structure in Figure S3 (a) and (b). Selected bond distances (Å) and bond angles (°) for [Cu – B] are summarized in Table S2. All the M – O distances are within the normal ranges allowing for statistical errors.[61,62]

In order to examine the thermal stability and bulk purity of the both coordination polymers [Cu – A] and [Cu – B] we have done thermogravimetric analyses (TGA) and powder X-ray diffraction patterns (PXRD). The details of these analyses are given in experimental section (supporting information).

Electrochemical measurements

Cyclic voltammetry (CV) measurements were obtained at bare GC, MWCNT/GC, [Cu–A], and [Cu–B] under N_2 (Figure S5) and O_2 (Figure 2) atmosphere in saturated 0.1 M KOH solution.

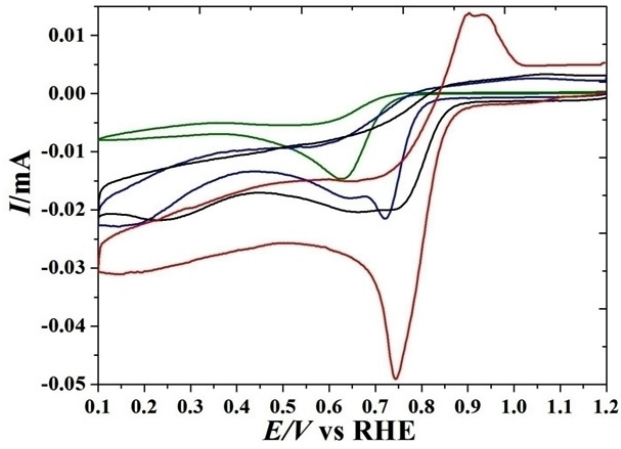

Figure 2. Cyclic voltammograms of GC (in green), MWCNT/GC (in blue), **[Cu–A]** (in red) and **[Cu–B]** (in black) performed in 0.1 M KOH, under saturated O_2 at 10 mV/s.

Figure S6 shows the CVs of individual catalyst under N_2 and O_2 saturated solutions. Anodic peaks for[Cu–B] under N_2 saturated electrolyte obtained at 0.92 V (peak I) and – 0.88 V (peak II) are attributed to Cu^0– Cu^{1+} and Cu^{1+}– Cu^{2+} oxidation processes, respectively. An anodic shift of 0.02 V in both of these anodic peaks were observed for [Cu–A] compared to those obtained for [Cu–B]. Furthermore cathodic peak attributed to Cu^{2+}– Cu^0 reduction at 0.7 and 0.72 V were observed for [Cu–B] and [Cu–A], respectively. The overall anodic shift of 0.02 V observed for [Cu–A] compared to [Cu–B] is likely due to the difference between ligands attached to the Cu active site. An increase in the cathodic current density compared to anodic current density was observed, which is also in good agreement with the assignment of redox processes involving two one–electron reduction and a two–electron oxidation processes, where the oxidation bands are assigned as one electron processes.

In comparison to MWCNT/GC, an anodic shift of 35 mV and 65 mV was observed for the ORR onset potentials obtained at the [Cu–B] and [Cu–A], respectively. The difference between onset potentials for ORR is likely due to the difference in the O_2 dissociation mechanism of these two compounds and change in the bonding energy of O_2 (or reduced intermediates) at the Cu active sites. The anodic current intensity was decreased remarkably under O_2 than the N_2atmosphere obtained for [Cu–B], which might be because of strong and almost irreversible bonding of O_2 or intermediates with the Cu site. The onset potential for ORR of the catalyst [Cu–A] is more anodic, thus, proving to be a better catalyst than the bare GC, MWCNT/GC, and [Cu–B]. In comparison with the Pt/C (Figure S4) onset potential at [Cu–A] is 100 mV cathodic (Figure S6C).

© 2017 Wiley-VCH Verlag GmbH & Co. KGaA, Weinheim

In order to confirm the effect of different ligands attached to Cu centre, kinetics of ORR was examined using RDE. LSVs of PtC/GC (Figure 3A), MWCNT/GC (Figure 3C), [Cu–A], (Figure 3E)

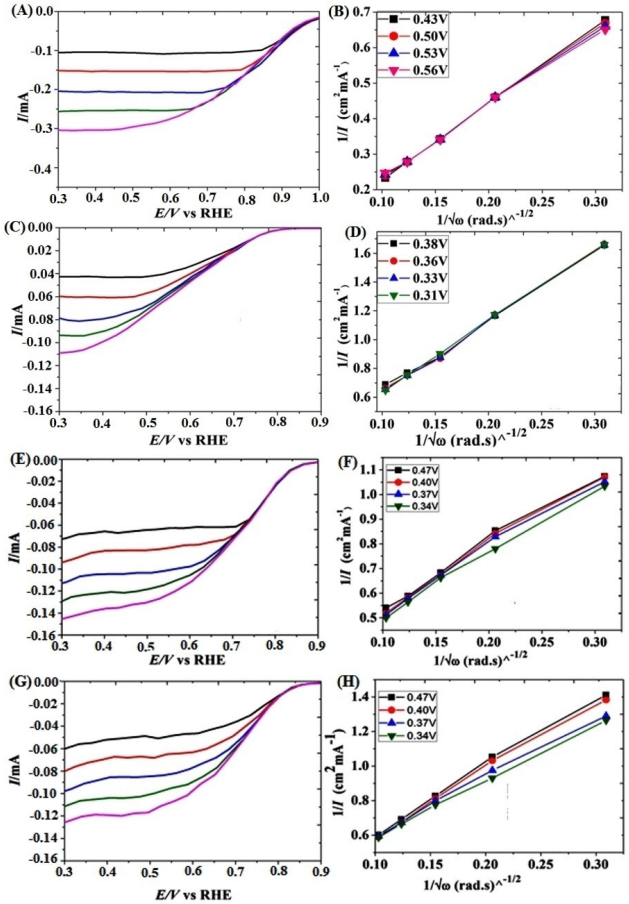

Figure 3. (A), (C),(E), (G) Linear sweep voltammetry of Pt/C/GC, MWCNT/GC, **[Cu–A]** and **[Cu–B]** performed with RDE in 0.1 M KOH, at different rpm 100 (in green), 225 (in red), 400 (in blue), 625 (in blue) and 900 (in black) under saturated O_2 at 10 mV/s *vs.* RHE. (B), (D), (F), (H) shows the Koutecky–Levich plot respective compounds.

and [Cu–B] (Figure 3G) were obtained at various rotation speeds from 100 to 900 rpm with a scan rate of 10 mV s^{-1}. Koutecky–Levich plots(K – L plot) were shown in (Figure 3 B, D, F and H), using the Koutecky–Levich Equation 1;

$$1/j = 1/j_k + 1/j_L = 1/j_k + 1/(B\omega^{1/2}) \quad (1)$$

where $B = 0.62nFCD^{2/3}v^{-1/6}$, j_k is the kinetic current density, j is the measured current density, j_L is the Levich current density, n is the number of electrons transferred per oxygen molecule, F is the Faraday constant i.e. 96,485 C mol^{-1}, C is the dissolved oxygen concentration in the solution (1.26 x 10^{-6}mol cm^{-3}), v is the kinematic viscosity of the solution (1.009 x 10^{-2} cm^2s^{-1}), D is the diffusion coefficient of oxygen (2.1 x 10^{-5} cm^2 s^{-1}), and ω is the rotation rate (rad s^{-1}). Assuming a four–electron reaction and the known geometric electrode surface area, the theoretical slope B is 2.5 cm^2 $rad^{1/2}$ mA^{-1} $s^{-1/2}$.

Based on the slope of the straight line from K–L plot, the number of electrons involved in the ORR were estimated to be 2.37 and 3.24 in the examined range of potential (0.4 to 0.8 V) for [Cu–B] and [Cu–A], respectively. It has been reported that the number of electrons can be affected due to loading density of catalyst.[63] Although, loading densities for both the catalysts (i.e. ca. 450 μg cm^{-1}) were well–above the limit to obtain four–electrons ORR (i.e. 200 μg cm^{-1}), lower number of electrons involved in the ORR is proposed due to an effect of different ligands attached to Cu active sites which results in to the different ORR pathways.

Figure S11 (A), (B), (C), and (D) was used to estimate Tafel slope and kinetic current density was determined from Equation 2:

$$j_k = (j \times j_L)/(j_L - j) \quad (2)$$

It has been assigned that the two slopes at low current density (LCD) and high current density (HCD) regions are representing the change of adsorption of reaction intermediates from Temkin to Langmurian conditions or because of the change in the surface coverage of OH, which influences the adsorption of O_2 molecules. The Tafel slopes (HCD/LCD) obtained for [Cu–A] (Figure S11C) and [Cu–B] (Figure S11D) are 122/83 and 131/84 mV dec^{-1}, respectively. The lower values of Tafel slope and higher kinetic current densities at the [Cu–A] clearly show that ORR is kinetically more enhanced compared to [Cu–B] (Table 1).

Table 1. Electrocatalytic parameters of **[Cu – A]** and **[Cu – B]**.

Electrode	Γnmol / cm^2	Onset potential /V vs. RHE	N	Tafel slope HCD/LCD mV/dec	$E_{1/2}$ at 400 rpm/ mV
[Cu – A]	11.03	0.866	3.24	122/83	741
[Cu – B]	5.5	0.834	2.37	131/84	701
MWCNT/ GC	–	0.8	2.0	185/96	620
Pt/C/GC	–	0.96	3.9	119/59	850

Based on the number electrons involved in the ORR, Tafel slopes and kinetic currents at the [Cu–A], two pathways of ORR mechanism can be predicted i.e. parallel ($k_1 = k_2$ and $k_3 = 0$) and serial ($k_2 = 2 \times k_3$ and $k_1 = 0$) pathways shown in Scheme 1.[64] However, these parameters estimated for the [Cu–B] demonstrates that the ORR probably follows the serial pathway ($k_2 = k_3$ and $k_1 = 0$) favourably with ca. 2 electron process.

The real surface coverage of electrocatalytically active catalyst (Γ) is estimated (Table 1) from the CVs measured at scan rates (v) from 5 to 100 mV s^{-1} (data used from the Figure S7, S9). Equation 3 is used to estimate the Γ.[65]

© 2017 Wiley-VCH Verlag GmbH & Co. KGaA, Weinheim

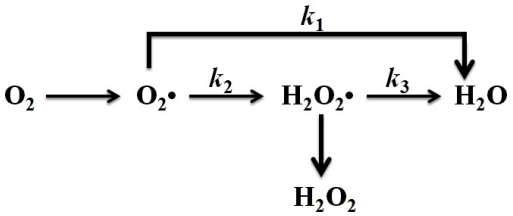

Scheme 1. ORR model proposed mechanism.

$$\Gamma = Q/nFA \quad (3)$$

where the amount of charge (Q) is calculated by the integration of area under the cathodic peak current for the reduction of Cu^{2+} to Cu^0 (corrected for the background current). Herein this relationship, n is the number of electrons involved in the redox reaction (n = 2 for this process), F is the Faraday constant, and A is the geometric electrode area (0.07068 cm^2). The Γ for [Cu–B] and [Cu–A] are 5.5 and 11.03, respectively. The Nicholson and Shain plot shows linearity with I vs. square root indicating the process is diffusion controlled at both catalysts (Figure S8, S10).

Along with the catalytic activity, stability is equally important for their practical applications. Thus, the stabilities of these catalysts were assessed by CV in the potential window of 0.1 to 1.1 V vs. RHE for consecutive 100 cycles under the N_2 saturated atmosphere. Figures S12 and S13 clearly demonstrate that [Cu–A] is more stable than the [Cu–B]. These results noticeably reveal that stability is drastically affected by the ligands. Further studies are going on to enhance its stability and to analyse an effect of other ligands on the Cu catalytic activity and their stabilities.

In the literature, examples of mononuclear and binuclear copper complex catalysts can be found for ORR, while the latter exhibits higher catalytic activity.[66] In the present study both [Cu–A] and [Cu–B] are mononuclear copper catalysts. Thus, it is noteworthy to compare the onset potential of [Cu–A] with the reported Cu-based catalysts (Table S3 Blue). The onset potential of [Cu–A] (0.866 V vs. RHE) is anodic compared with other reported mononuclear Cu-based catalysts such as CuINPD/C, copper phenolato complex bearing a pyrene group immobilized CNT, CNTs + TAmPyCu, [Cu(tripic)(NCMe)]PF6, and rGO + TAmPyCu which proves the best ORR catalyst among all these catalysts. However, its onset potential is cathodic to the Cu catalyst covalently attached to the carbon substrates (i.e. CNTs–TAmPyCu and rGO–TAmPyCu), most probably due to the synergistic effect of graphitic carbon surface towards ORR. The number of electrons involved in the ORR catalysis on the [Cu–A] is in agreement with the physisorbed mononuclear copper catalysts (ca. 3.2). These findings clearly show that [Cu–A] catalyses ORR with low overpotential. The onset potentials and the number of electrons involved in the ORR are also compared with binuclear copper catalysts which proved to be efficient than the [Cu–A]. These binuclear copper catalysts are proved to be efficient due to the bimetallic active site which catalyses the ORR through the formation of Cu–OOH specie. This mechanism is totally different than the catalysis on the [Cu–A] and [Cu–B], which is expected to follow through the paddle-wheel mechanism as proposed earlier.[60] Therefore, lower number electrons involved in the ORR at the [Cu–A] than these binuclear copper catalysts is expected. To summarize, among the mononuclear copper catalysts [Cu–A] shows more anodic onset potential with 3.24 number of electrons involved in the ORR.

Conclusions

In this study, an influence of the acetate and benzoate ligands attached Cu on an electrochemical ORR catalysis and stability has been realized. These results clearly demonstrate that [Cu–A] is thermodynamically and kinetically more favourable than [Cu–B] towards ORR. Although both catalysts have the same type of active metal site different ligands attached to Cu centre can change the catalytic ORR activity and stability. The enhanced catalytic activity observed for [Cu–A] compared to [Cu–B] could be attributed to two factors: i) Given the same amount of catalysts, [Cu–A] contains more active sites than [Cu–B] since it has lower molecular weight as a result of lighter bridging groups in paddle–wheel units. Chains in [Cu–A] are much closer to each other, which results in a higher number of copper sites per volume. ii) Although copper sites in both systems adopt square pyramidal geometry they have slightly different coordination environments proven by the comparison of Cu···Cu distances and O–Cu–O bond angles. The study herein implies that such small changes in the coordination environment of the active metal site, which is originated from the type of bridging unit, could lead to significant changes in the catalytic activity. This study demonstrates the possibility of tuning the ligands attached to Cu centre further can provide us catalysts that can replace platinum in future.

Supporting information

Detailed experimental, crystal structure and their characterization i.e. TGA, XRD, FTIR electrochemical measurements and stability are summarized in the supporting information.

Acknowledgments

The authors thank to the Science and Technology Council of Turkey, TUBITAK for financial support (214Z095). Bhushan Patil also thanks to TUBITAK for financial support (Project number: 115M375).

Conflict of Interest

The authors declare no conflict of interest.

Keywords: Copper coordination polymers · Ligand effect · ORR catalyst

[1] S. C. Barton, J. Gallaway, P. Atanassov, *Chem. Rev.* **2004**, *104*, 4867–4886.
[2] A. Le Goff, M. Holzinger, S. Cosnier, *Cell. Mol. Life Sci.* **2015**, *72*, 941–952.

© 2017 Wiley-VCH Verlag GmbH & Co. KGaA, Weinheim

[3] M. Rasi, L. Rajendran, M. V. Sangaranarayanan, *J. Electrochem. Soc.* **2015**, *162*, H671–H680.
[4] J. Yang, J. Hu, M. Weng, R. Tan, L. Tian, J. Yang, J. Amine, J. Zheng, H. Chen, F. Pan, *ACS Appl. Mater. Interfaces* **2017**, *9*, 4587–4596.
[5] S. S. Shinde, C.–H. Lee, A. Sami, D.–H. Kim, S. U. Lee, J.–H. Lee, *ACS Nano* **2016**,*11*, 347–357.
[6] Y. Wang, G. Li, J. Jin, S. Yang, *Int. J. Hydrogen Energy* **2017**, *42*, 5938–5947.
[7] G. He, Y. Song, K. Liu, A. Walter, S. Chen, S. Chen, *ACS Catal.* **2013**, *3*, 831–838.
[8] V. Malgras, H. Ataee-Esfahani, H. Wang, B. Jiang, C. Li, K. C.-W. Wu, J. H. Kim, Y. Yamauchi, *Adv. Mater.* **2016**, *28*, 993–1010.
[9] C. Li, T. Sato, Y. Yamauchi, *Angew. Chem. Int. Ed.* **2013**, *52*, 8050–8053.
[10] B. Jiang, C. Li, V. Malgras, M. Imura, S. Tominaka, Y. Yamauchi, *Chem. Sci.* **2016**, *7*, 1575–1581.
[11] S. Cosnier, R. Haddad, D. Moatsou, R. K. O'Reilly, *Carbon N. Y.* **2015**, *93*, 713–718.
[12] C.–Y. Su, B.–H. Liu, T.–J. Lin, Y.–M. Chi, C.–C. Kei, K.–W. Wang, T.–P. Perng, *J. Mater., Chem. A* **2015**, *3*, 18983–18990.
[13] A. Navaee, A. Salimi, *J. Mater. Chem. A* **2015**, *3*, 7623–7630.
[14] M. Klingele, C. Pham, K. R. Vuyyuru, B. Britton, S. Holdcroft, A. Fischer, S. Thiele, *Electrochem. commun.* **2017**, *77*, 71–75.
[15] H. R. Byon, J. Suntivich, Y. Shao–Horn, *Chem. Mater.* **2011**, *23*, 3421–3428.
[16] A. N. Oldacre, A. E. Friedman, T. R. Cook, *J. Am. Chem. Soc.* **2017**,*139*, 1424–1427.
[17] G. Passard, A. M. Ullman, C. N. Brodsky, D. G. Nocera, *J. Am. Chem. Soc.* **2016**, *138*, 2925–2928.
[18] W. Zhang, T. Cui, L. Yang, C. Zhang, M. Cai, S. Sun, Y. Yao, X. Zhuang, F. Zhang, *J. Colloid Interface Sci.* **2017**, *497*, 108–116.
[19] Q. Lai, L. Zheng, Y. Liang, J. He, J. Zhao, J. Chen, *ACS Catal.* **2017**,*7*, 1655–1663.
[20] C. Li, Z. Chen, Y. Ni, F. Kong, A. Kong, Y. Shan, *J. Mater. Chem. A* **2016**, *4*, 14291–14297.
[21] E. Meku, C. Du, Y. Sun, L. Du, Y. Wang, G. Yin, *J. Electrochem. Soc.* **2016**, *163*, F132–F138.
[22] E. C. M. Tse, D. Schilter, D. L. Gray, T. B. Rauchfuss, A. A. Gewirth, *Inorg. Chem.* **2014**, *53*, 8505–8516.
[23] C. Liu, H. Lei, Z. Zhang, F. Chen, R. Cao, *Chem. Commun.* **2017**, *53*, 3189–3192.
[24] S. Kim, A. D. Siewe, E. Lee, H. Ju, I. H. Park, K. M. Park, M. Ikeda, Y. Habata, S. S. Lee, *Inorg. Chem.* **2016**, *55*, 2018–2022.
[25] S. E. H. Etaiw, A. S. Badr El–Din, S. N. Abdou, *Transit. Met. Chem.* **2016**, *41*, 413–425.
[26] X. Luo, Y. Cao, T. Wang, G. Li, J. Li, Y. Yang, Z. Xu, J. Zhang, Q. Huo, Y. Liu, M. Eddaoudi, *J. Am. Chem. Soc.* **2016**, *138*, 786–789.
[27] S. Hazra, M. F. C. Guedes Da Silva, A. Karmakar, A. J. L. Pombeiro, *RSC Adv.* **2015**, *5*, 28070–28079.
[28] M. Rancan, J. Tessarolo, S. Quici, L. Armelao, *Chem. Commun.* **2014**, *50*, 13761–13764.
[29] W.–J. Hu, L.–Q. Liu, M.–L. Ma, X.–L. Zhao, Y. A. Liu, X.–Q. Mi, B. Jiang, K. Wen, *Inorg. Chem.* **2013**, 9309–9319.
[30] M. Kallitsakis, E. Loukopoulos, A. Abdul–Sada, G. J. Tizzard, S. J. Coles, G. E. Kostakis, I. N. Lykakis, *Adv. Synth. Catal.* **2016**, *359*,138–145.
[31] Z. Ma, A. V. Gurbanov, M. Sutradhar, M. N. Kopylovich, K. T. Mahmudov, A. M. Maharramov, F. I. Guseinov, F. I. Zubkov, A. J. L. Pombeiro, *J. Mol. Catal. A Chem.* **2016**, *428*, 17–23.
[32] W. Zhang, F. Wang, S. D. McCann, D. Wang, P. Chen, S. S. Stahl, G. Liu, *Science* **2016**, *353*, 1014–1018.
[33] J.–M. Li, Y.–H. Wang, Y. Yu, R.–B. Wu, J. Weng, G. Lu, *ACS Catal.* **2017**, *7*, 2661–2667.
[34] Y. Li, *J. Phys. Org. Chem.*, 2016, 1–8.
[35] M.–G. Alexandru, D. Visinescu, S. Shova, F. Lloret, M. Julve, *Inorg. Chem.* **2017**, *56*, 2258–2269.
[36] M. Almáši, V. Zeleňák, A. Zeleňáková, Z. Vargová, I. Císařová, *Inorg. Chem. Commun.* **2016**, *74*, 66–71.
[37] J.–W. Zhang, X.–L. Li, X.–M. Kan, H. Wu, Y. Liu, B.–Q. Liu, *CrystEngComm* **2017**, *19*, 661–668.
[38] C. Q. Jiao, Z. Zhao, C. Ma, Z. G. Sun, D. P. Dong, Y. Y. Zhu, J. Li, *Cryst. Growth Des.* **2016**, *16*, 5624–5635.
[39] X. Liu, F. Li, X. Ma, P. Cen, S. Luo, Q. Shi, S. Ma, Y. Wu, C. Zhang, Z. Xu, W. Song, G. Xie, S. Chen, *Dalt. Trans.* **2016**, 1207–1217.
[40] V. G. Vegas, R. Lorca, A. Latorre, K. Hassanein, C. J. Gómez–García, O. Castillo, Á. Somoza, F. Zamora, P. Amo–Ochoa, *Angew. Chemie Int. Ed.* **2017**, *56*, 987–991.
[41] J. Li, W. Y. Huang, S. S. Qian, Q. Y. Li, H. L. Zhu, *InorganicaChim. Acta* **2015**, *435*, 16–24.
[42] P. Huang, F. Wu, L. Mao, *Anal. Chem.* **2015**, *87*, 6834–6841.
[43] N. Sahu, D. Das, S. Mondal, S. Roy, P. Dutta, N. Sepay, S. Gupta, E. López–Torres, C. Sinha, *New J. Chem.* **2016**, *40*, 5019–5031.
[44] M. V Girgaonkar, S. G. Shirodkar, *Res. J. Recent. Sci.* **2012**, *1*, 110–116.
[45] J.–W. Cui, W.–J. An, K. Van Hecke, G.–H. Cui, *Dalt. Trans.* **2016**, *45*, 17474–17484.
[46] B. Zhou, L.–M. Liang, J. Yao, *J. Solid State Chem.* **2015**, *223*, 152–155.
[47] Q. Liu, X. Liu, C. Shi, Y. Zhang, X. Feng, M.–L. Cheng, S. Su, J. Gu, *Dalt. Trans.* **2015**, *44*, 19175–19184.
[48] Y.–T. Xi, P.–J. Wei, R.–C. Wang, J.–G. Liu, *Chem. Commun.* **2015**, *51*, 7455–7458.
[49] J. Wang, K. Wang, F.–B. Wang, Xing–Hua Xia, *Nature Commun.* **2014**, 1–9.
[50] N. Dimcheva, T. Dodevska, E. Horozova, *J. Electrochem. Soc.* **2013**, *160*, 414–419.
[51] G. Göbel, T. Dietz, F. Lisdat, *Electroanalysis* **2010**, *22*, 1581–1585.
[52] S. Tsujimura, Y. Kamitaka, K. Kano, *Fuel Cells*, **2007**, *6*, 463–469.
[53] D. Li, T. Okajima, L. Mao, T. Ohsaka, *Int. J. Electrochem. Sci.* **2014**, *9*, 1390–1398.
[54] F. Tasca, D. Farias, C. Castro, C. Acuna–Rougier, R. Antiochia, *PLOS One* **2015**, *10*, 1–9.
[55] Y. Yang, H. Zeng, W. S. Huo, Y. H. Zhang, *J. Inorg. Organomet. Polym. Mater.* **2017**, *27*, 201–214.
[56] S. Patra, S. Sene, C. Mousty, C. Serre, A. Chauss, L. Legrand, N. Steunou, *ACS Appl. Mater. Interfaces* **2016**, *8*, 20012–20022.
[57] Y. Zhou, Y. Umasankar, R. P. Ramasamy, *J. Electrochem. Soc.* **2015**, *162*, H911–H917.
[58] N. Lalaoui, R. David, H. Jamet, M. Holzinger, A. Le Goff, S. Cosnier *ACS Catal.* **2016**, *6*, 4259–4264.
[59] M. Bourourou, K. Elouarzaki, N. Lalaoui, C. Agnès, A. Le Goff, M. Holzinger, A. Maaref, S. Cosnier, *Chem. – A Eur. J.* **2013**, *19*, 9371–9375.
[60] R. Mishra, E. Ülker, F. Karadas, *ChemElectroChem* **2017**, 75–80.
[61] K. Takahashi, N. Hoshino, T. Takeda, S. I. Noro, T. Nakamura, S. Takeda, T. Akutagawa, *Inorg. Chem.* **2015**, *54*, 9423–9431.
[62] Z. Staszak, A. Krojcer, M. Kubiak, A. Puszko, G. Maciejewska, M. Cieślak–Golonka, *Struct. Chem.* **2010**, *21*, 305–313.
[63] C. Retna Raj, T. Ohsaka, A. Samanta, S. H. Noh, S. Mondal, T. Okajima, *J. Mater. Chem. A* **2016**, *4*, 11156–11178.
[64] A. Damjanov, M. A. Genshaw, J. O. Bockris, *J. Chem. Phys.* **1966**, *45*, 4057.
[65] B. Patil, Y. Kobayashi, S. Fujikawa, T. Okajima, L. Mao, T. Ohsaka, *Bioelectrochemistry* **2014**, *95*, 15–22.
[66] S. Gentil, D. Serre, C. Philouze, M. Holzinger, F. Thomas, A. L. Goff, *Angew. Chem. Int. Ed.* **2016**, *55*, 2517 – 2520.

Submitted: June 11, 2017
Revised: August 31, 2017
Accepted: September 5, 2017

© 2017 Wiley-VCH Verlag GmbH & Co. KGaA, Weinheim